Inhibition of The hERG Potassium Channel By The Polycyclic Aromatic Hydrocarbon Pollutant Phenanthrene

Ehab Al-Moubarak
University of Bristol
Holly A. Shiels
University of Manchester School of Medicine: The University of Manchester Faculty of Biology Medicine and Health
Yihong Zhang
University of Bristol
Chunyun Du
University of Bristol
Oliver Hanington
University of Bristol
Stephen C. Harmer
University of Bristol
Christopher E. Dempsey
University of Bristol
Jules Hancox (✉ jules.hancox@bristol.ac.uk)
University of Bristol https://orcid.org/0000-0002-2055-6482

Research Article

Keywords: hERG, hydrocarbon, PAH, phenanthrene, pollutant, potassium channel

Posted Date: July 14th, 2021

DOI: https://doi.org/10.21203/rs.3.rs-680612/v1

Version of Record: A version of this preprint was published at Cellular and Molecular Life Sciences on November 2nd, 2021. See the published version at https://doi.org/10.1007/s00018-021-03967-8.

Abstract

The lipophilic polycyclic aromatic hydrocarbon (PAH) phenanthrene is relatively abundant in polluted air and water and can access and accumulate in human tissue. Phenanthrene has been reported to interact with cardiac ion channels in several fish species. This study was undertaken to investigate the ability of phenanthrene to interact with *hERG* (*human Ether-à-go-go-Related Gene*) encoded K^+ channels, which play a central role in human ventricular repolarization. Pharmacological inhibition of hERG can be proarrhythmic. Whole-cell patch clamp recordings of hERG current (I_{hERG}) were made from HEK293 cells expressing wild-type (WT) and mutant hERG channels. WT I_{hERG1a} was inhibited by phenanthrene with an IC_{50} of 16.8 ± 1.7 μM, whilst $I_{hERG1a/1b}$ exhibited an IC_{50} of 1.8 ± 0.3 μM. WT I_{hERG} block showed marked voltage and time-dependence, indicative of dependence of inhibition on channel gating. The inhibitory effect of phenanthrene was markedly impaired by the attenuated-inactivation N588K mutation. Remarkably, mutations of S6 domain aromatic amino acids (Y652, F656) in the canonical drug binding site did not impair the inhibitory action of phenanthrene; the Y652A mutation augmented I_{hERG} block. In contrast, the F557L (S5) and M651A (S6) mutations impaired the ability of phenanthrene to inhibit I_{hERG}, as did the S624A mutation below the selectivity filter region. Computational docking using a cryo-EM derived hERG structure supported the mutagenesis data. Thus, phenanthrene acts as an inhibitor of the hERG K^+ channel by directly interacting with the channel, binding to a distinct site in the channel pore domain.

Introduction

Humanity's dependence on fossil fuels has led to the near-ubiquitous pollution of the environment with petrochemicals. Exposure to polluted air is associated with a range of adverse cardiovascular events including heart attacks, strokes, and irregular heart rhythms, particularly in people already at risk for these conditions [1]. The mechanisms of cardiotoxicity are complex and can be attributed in part, to nanoparticles containing aromatic hydrocarbons (PAHs) that are produced during combustion of coal, petroleum, diesel, tobacco, and by cooking food [1]. The adverse health effects of PAHs have long been recognized, but with a focus primarily on carcinogenic compounds such as benzo(a)pyrene (BAP) [2] and other larger molecular weight members (i.e., 4 + rings) of the PAH family. In contrast, the non-carcinogenic smaller PAHs have largely been ignored by the human biomedicine community. These smaller 2- and 3-ring compounds are several orders of magnitude more abundant than the larger 4-ring + PAHs in the fossil fuel sources that feed urban air pollution [3] but are not routinely measured in air pollution; when they are, their ubiquity and abundance are clear. Other than 2-ringed naphthalenes, phenanthrene with 3-rings and its alkylated homologs make up the largest fraction of the measured PAHs in virtually all fuel-related sources. This includes fine particulate matter (e.g., $PM_{2.5}$) such as diesel exhaust particles and broadly collected urban $PM_{2.5}$ (e.g. [4;5]. More importantly, phenanthrenes are volatile so are even more abundant in the vapor phase of vehicle exhaust and urban air (e.g. [6;7].

While the phenanthrenes (and other smaller PAHs) have not been considered fully in the etiology of air pollution-related cardiovascular disease in humans, for nearly three decades they have been a major focus of the cardiotoxicity syndrome that occurs in developing fish following aquatic oil spills (reviewed in [8]. Oil spills such as the 1989 Exxon Valdez tanker grounding and the 2010 Deepwater Horizon wellhead blowout released large quantities of PAHs directly into the marine environment, bringing global attention to the cardiotoxic effects of PAHs for fish [1;9;10]. Exposure of zebrafish embryos to 3-ringed PAHs was found to produce bradycardia and arrhythmia consistent with atrioventricular block; the authors suggested *Ether-à-go-go-Related Gene* (ERG) encoded K^+ channels as a potential target that might mediate such effects [9]. Crude oil extracts from the Deepwater Horizon disaster were then shown to exert direct effects on the function of tuna cardiac myocytes: they produced impairment of calcium cycling and action potential prolongation, associated with inhibition of the rapid delayed rectifier K^+ current (I_{Kr}, the ion current carried by *erg* [11]). Subsequent work isolated the 3-ringed PAH phenanthrene as the key moiety involved in these effects producing a concentration-dependent ventricular action potential prolongation and inhibition of I_{Kr} [12]. Phenanthrene has subsequently been shown to increase sodium current and reduce both calcium current and I_{Kr} in ventricular myocytes from rainbow trout [13], with ventricular action potential prolongation and reductions in calcium current and I_{Kr} with phenanthrene also recently reported for brown trout cardiomyocytes [14]. Furthermore, phenanthrene has recently been reported to inhibit calcium current and I_{Kr} in zebrafish cardiomyocytes [15]. There is debate as to whether toxic effects of pollutants on fish from crude oil may largely result from membrane disruption rather than interaction with specific receptors (e.g. [16]. Whilst the effects of phenanthrene on specific cardiac ion channel currents may be consistent with a direct rather than non-selective effect, definitive evidence for this is currently lacking.

The reported effects of phenanthrene on fish I_{Kr} are of relevance to human cardiovascular health because I_{Kr} is known to be of key importance not only in animal model species, but also to normal human ventricular repolarization [17;18]. I_{Kr} channels normally exist as homo-tetramers of pore-forming subunits encoded by *hERG* (*human Ether-à-go-go-Related Gene*, alternative nomenclature *KCNH2*; [19;20]. Loss- and gain- of function mutations to *hERG* respectively underlie forms of inherited Long and Short QT Syndromes (LQTS and SQTS, respectively) [19;21]. Moreover, due to unique structural features, hERG channels are highly susceptible to pharmacological blockade, leading to a drug-induced form of LQTS, with its associated risk of dangerous ventricular arrhythmias [17;18]. Phenanthrene is relatively abundant in polluted air and water. It is lipophilic and can access and accumulate in human tissue via skin and mucus membranes [1]. Given the known susceptibility of hERG to pharmacological blockade and the fact that fish I_{Kr} is inhibited by phenanthrene, it is reasonable to expect that hERG itself may be susceptible to phenanthrene inhibition. Furthermore, alignment of fish ERG and hERG sequences reveals a high level of identity in regions of the channel that constitute the canonical drug binding site (Fig. 1A and [1]). It therefore seems likely that human I_{Kr}/hERG also may be susceptible to inhibition by phenanthrene. Accordingly, this study was undertaken: (i) to determine the propensity or otherwise of phenanthrene to inhibit ionic current (I_{hERG}) carried by recombinant hERG channels; (ii) to explore the underlying

mechanism of any observed effect. Some of this work has been published in meeting abstract form [22;23].

Materials And Methods

Maintenance of mammalian cell lines and cell transfection

As in previous studies (e.g. [24–26], experiments were performed on HEK293 cells stably expressing WT hERG [27] or transiently transfected with hERG mutant cDNAs. The hERG stable-line was generously provided by Professor Craig January [27]. HEK293 cells (ECACC, Porton Down, UK) were transiently transfected with cDNA plasmids using Lipofectamine 2000 (Invitrogen, Paisley, UK) according to the manufacturer's instructions. Expression plasmid encoding CD8 was also added (in pIRES, donated by Dr I Baró, University of Nantes, France) as a marker for successful transfection. Cells were passaged using enzyme free cell dissociation solution (Millipore, Watford, UK) and plated onto sterilized shards of glass coverslips in 40-mm petri dishes containing a modification of Dulbecco minimum essential medium with Glutamax-1 (DMEM; Invitrogen, Paisley, UK). This was supplemented with 10% fetal bovine serum (Gibco, Gloucester, UK), 50 µg/mL gentamycin (Invitrogen, Paisley, UK), and 400 µg/mL geneticin (G418, Invitrogen, Paisley, UK) for the WT hERG-expressing line. For experiments utilizing cells transiently transfected with hERG mutants, recordings were performed 12-72h after transfection. Successfully transfected cells (positive to CD8) were identified using Dynabeads® (Invitrogen, Paisley, UK) [25;26]. The N588K, S624A, Y652A, M651A and F557L mutations to hERG1a have all been used in prior studies from our laboratory (e.g. [24–26;28];[29], as has hERG1a/1b co-expression [25;30]. Zebrafish ERG (zERG) was synthesised and provided in pcDNA3.1 by Genscript (Leiden, Netherlands; NCBI Reference Sequence: NM_212837.1).

The F656V mutation was made to hERG1a as described in [31]. F656T was made using QuikChange (Agilent) mutagenesis using conditions described in [31] and the following primer sequences:

forward – 5’-GTATGCTAGCATCACCGGCAACGTGTCG-3’

reverse – 5’- CGACACGTTGCCGGTGATGCTAGCATAC-3’

Experiments were performed on hERG1a current (I_{hERG1a}) except for the data in Fig. 2B and C, which were conducted using co-expressed hERG1a and 1b channels ($I_{hERG1a/1b}$), and supplementary Fig. 2 which shows data from zERG (I_{zERG}).

Electrophysiological recording

Recordings were made as described previously [25;26]. In brief, electrophysiological recordings were made at least 24 hrs after transfection, using an Axopatch 200B amplifier (Molecular Devices) with a CV-4/100 headstage and data acquisition via a Digidata 1320 interface (Molecular Devices). Glass shards with plated HEK293 cells were placed in the recording chamber of an inverted microscope (Nikon Diaphot,

USA). The extracellular superfusate was a standard Tyrode's solution containing (in mM): 140 NaCl, 4 KCl, 2.5 $CaCl_2$, 1 $MgCl_2$, 10 glucose, and 5 HEPES (titrated to pH 7.4 with NaOH) [24–26]. Patch pipettes (AM-systems Inc, USA) had resistances of 2–4 MΩ and were filled with a solution containing (in mM): 130 KCl, 1 $MgCl_2$, 5 EGTA, 5 MgATP and 10 HEPES (titrated to pH 7.2 with KOH) [24–26]. Series resistance was typically compensated by 60–80%. Currents were filtered at 1–5 kHz depending on the voltage protocol used and were digitized at 10 kHz. All measurements were made at room temperature (21 ± 1^{o}C). Room temperature was employed to facilitate accurate evaluation of phenanthrene effects because in pilot experiments at 37^{o}C, stability of phenanthrene-containing superfusate appeared variable. It also facilitated comparison of phenanthrene blocking potency between human and zebrafish ERG data in this study and with prior recordings from fish myocytes conducted at room temperature [11–13].

Trafficking assay.

Evaluation of the effects of 3 and 30 μM phenanthrene on hERG channel trafficking was performed using a *LI-COR* based In-Cell/On-Cell Western assay, as described previously [32] see online supplement for more details).

Phenanthrene

Phenanthrene was obtained from Merck (Sigma-Aldrich) and dissolved in DMSO to give stock solutions of 20, 30 and 50 mM. Experimental solutions with phenanthrene concentrations shown in the Results contained a maximum of 0.1% DMSO.

Computational Docking

Docking of phenanthrene to hERG was initially performed using the cryo-EM derived structure for hERG [33] (PDB code 5VA2), as described previously [26;29;34]. A model closely related to the cryo-EM structure was obtained from a short molecular dynamics (MD) simulation in which the F656 side chain of one of the four hERG subunits was found to reorient towards the pore – this subunit was then replicated around all four pore subunits to produce a model with all four F656 side chains facing the pore; this structure was used for the docking data shown in Fig. 6. The phenanthrene structure was converted from SMILE representation (obtained from PubChem database) to a 3D structure, hydrogens were added and the molecule energy minimised.

Phenanthrene was docked in the hERG structure and in the related model using GOLD (GOLD version 5.6; Cambridge Crystallographic Data Centre, Cambridge, UK). The central pore cavity was initially chosen as a binding site where a radius of 10 angstrom extended from the centre of the cavity and in a level with a middle point between the canonical aromatic residues F656 and Y652. The side chains of these aromatic residues were set to be freely flexible during docking simulations. Rotamer sampling was maximally set to 300,000 generations. Dockings were scored by Goldscore and rescored by Chemscore. Two hundred docking repeats were made in each case and the low-energy-score poses were selected and inspected. Phenanthrene was also docked within a side pocket under the selectivity filter in the open pore F656-

rotated hERG model. This binding pocket was centred above the β-carbon of Y652 and encompassed a volume having a radius of 7 angstrom. Within this selection, the side chains for the following residues from subunit A of the tetrameric channel were permitted to rotate freely: F557, L622, T623, S624, L650, M651, Y652, I655. F656 side chains from adjacent subunits (A and B) of the channel were also allowed to rotate freely. Similar setting and parameters were used as above where also 200 docking repeats for each drug were generated and low energy poses identified.

Results were presented using PyMOL Molecular Graphics System, Version 2.0 Schrödinger, LLC.

Data presentation and analysis

Data are presented as mean ± SEM of the number of independent experiments indicated (*n*). Statistical comparisons were made using a Student *t* test, one- or two-way analysis of variance (ANOVA) followed by a Bonferroni or Dunnett's post-test, as appropriate. *P* values < 0.05 were considered to be statistically significant.

Fractional block of hERG current (I_{hERG}) by the different phenanthrene (Phen) concentrations studied was determined using the equation:

$$\text{Fractional block} = 1-((I_{hERG\ -Phen})/I_{hERG\ -Control}) \quad (1)$$

Where "Fractional block" refers to the degree of inhibition of hERG current by a given concentration of phenanthrene. $I_{hERG^-\ Phen}$ and $I_{hERG-Control}$ represent current amplitudes in the presence and absence of phenanthrene.

Concentration-response data were fitted by a standard Hill equation of the form:

$$\text{Fractional block} = 1/(1+(IC_{50}/[Phen])^{\ h}) \quad (2)$$

Where IC_{50} is [Phen] producing half-maximal inhibition of the I_{hERG} tail and *h* is the Hill coefficient for the fit.

Half maximal activation voltages for I_{hERG} were obtained from current-voltage (I-V) relations from I_{hERG} tails measured at -40 mV in the absence or presence of phenanthrene following voltage commands to different test potentials, using the following Boltzmann equation:

$$I = I_{max}/1 + \exp((V_{0.5}-Vm)/k) \quad (3)$$

where $I = I_{hERG}$ tail amplitude following test potential V_m, I_{max} is the maximal I_{hERG} tail observed during the protocol, $V_{0.5}$ is the half maximal activation voltage of I_{hERG} and *k* is the slope factor describing I_{hERG} activation.

Voltage-dependent activation curves were constructed by calculating activation variables at 2 mV intervals between − 80 mV and + 40 mV. Values for $V_{0.5}$ and *k* were derived from experimental fits to I-V data using Eq. (3) were inserted into the following equation:

Activation parameter = 1/1 + exp(($V_{0.5}$-Vm)/*k*) (4)

where the 'activation parameter' at test potential Vm lies between 0 and 1 and $V_{0.5}$ and *k* have the meanings described above for Eq. 3.

Results

WT I_{hERG} inhibition by phenanthrene

The sensitivity of I_{hERG} to inhibition by phenanthrene was determined using the protocol shown in Fig. 1B. This was comprised of a 2 s depolarization from − 80 mV to + 20 mV, followed by repolarization to -40 mV, at which the resurgent tail current that is typical of hERG was observed. I_{hERG} tail magnitude was measured relative to current elicited by a brief (50 ms) pulse from − 80 to -40 mV that preceded the 2 s voltage command. This protocol has been used in multiple prior studies of I_{hERG} pharmacology from our laboratory (e.g. [24–26;35]. Figure 1B shows exemplar records of I_{hERG} in control solution, the presence of 10 μM phenanthrene and following washout, whilst Fig. 1C shows a continuous plot of I_{hERG} tail amplitude during the experiment from which these example traces were taken. Phenanthrene application led to a progressive decline in I_{hERG} amplitude, which was largely reversible on washout. Five concentrations of phenanthrene, ranging from 1 μM to 50 μM, were tested in similar experiments. Higher concentrations could not be investigated due to issues with phenanthrene solubility and exposure of cells to higher levels of solvent. Fractional inhibition of I_{hERG} tails at each phenanthrene concentration was ascertained using Eq. 1 and values from different experiments at each concentration pooled to produce the concentration response plot shown in Fig. 1D. These data were fitted with Eq. 2, which yielded a half-maximal inhibitory concentration (IC_{50}) of 16.8 ± 1.7 μM and Hill slope: of 1.0 ± 0.1. It is apparent from the traces shown in Fig. 1B that in addition to reducing I_{hERG} amplitude, phenanthrene altered the deactivation time-course of the I_{hERG} tail. This effect was quantified by standard biexponential fitting of deactivating I_{hERG} tails at -40 mV following 2 s duration commands to + 20 mV. As shown in Fig. 2A, both fast and slow time-constants of deactivation (τ_f and τ_s) were significantly decreased in the presence of phenanthrene, whilst the proportion of deactivation described by τ_f increased. These findings indicate that phenanthrene application resulted in significant acceleration of I_{hERG} deactivation. Evaluation of the effects of chronic (24 hour) treatment of 3 and 30 μM phenanthrene on hERG1a channel trafficking showed no significant reduction in surface hERG protein expression by either concentration (see online Supplementary Fig. 1). In contrast, chronic treatment with 20 μM tamoxifen significantly reduced the level of surface hERG channel expression as has been previously reported [36] (online Supplementary Fig. 1). In additional comparative experiments on zebrafish hERG (Supplementary Fig. 2), phenanthrene inhibited I_{zERG} with an IC_{50} of 8.7 ± 0.93 μM (Hill co-efficient of 0.84 ± 0.09) and accelerated I_{zERG} deactivation.

There is evidence that native mammalian I_{Kr} channels are comprised of hERG1a together with the abbreviated hERG1b isoform, which possesses a shorter and distinct N terminus and which exhibits faster deactivation compared to hERG1a [37–39]. Figure 2Bi shows the effect of 10 μM phenanthrene on co-expressed hERG1a/1b current ($I_{hERG1a/1b}$). This concentration produced a marked reduction in $I_{hERG1a/1b}$ amplitude. In all, four phenanthrene concentrations (1–30 μM) were tested against $I_{hERG1a/1b}$ (Fig. 2Bii), yielding an IC_{50} value of 1.8 ± 0.3 (Hill coefficient 0.79 ± 0.11). Figure 2C shows the effect of 1 μM phenanthrene on deactivation time-constants of $I_{hERG1a/1b}$. Whilst, as expected, the rate of deactivation in control solution was faster for $I_{hERG1a/1b}$ than I_{hERG1a} alone (compare Fig. 2C with Fig. 2A), in contrast to the observed effect on I_{hERG} carried by hERG1a alone, phenanthrene application did not lead to a significant reduction in either fast or slow deactivation time-constant for $I_{hERG1a/1b}$, although the contribution of the fast component of deactivation was slightly greater in the presence of phenanthrene.

Inhibition by phenanthrene of I_{hERG} elicited at different voltages

Voltage-dependence of hERG inhibition was investigated for hERG1a using the I-V protocol shown in Fig. 3Ai, ii. This protocol was similar to that used in Fig. 1, but incorporated progressively larger depolarizations (in 10 mV increments) to test potentials between − 30 and + 60 mV. Whilst both pulse and tail I_{hERG} with voltage commands to more positive membrane potentials in the range tested were reduced by phenanthrene (10 μM), at more negative voltages in the tested range, the current appeared to increase in amplitude in the presence of phenanthrene. Figures 3B and 3C show normalized I-V relations for end-pulse current (Fig. 2B) and tail current (Fig. 2C). As Fig. 3B shows, the end-pulse I-V relation showed the bell-shape characteristic of I_{hERG} in both control and phenanthrene containing solutions; however, this appeared to be somewhat leftward shifted in phenanthrene compared to control. Superimposed on the same voltage axes is a plot of fractional block of I_{hERG} at each voltage. As is clearly illustrated, at potentials below + 10 mV negative fractional inhibition (representing an increase in current) of I_{hERG} was observed. This gave way to a progressive increase in end pulse current block, up to ~ + 40 mV. Normalized I_{hERG} tails were plotted and fitted with Eq. 4 in Fig. 3C, along with a superimposed plot of fractional inhibition. For all test potentials negative to ~ 0 mV, a fractional increase in I_{hERG} tail amplitude at -40 mV was seen, whilst fractional inhibition increased markedly up to ~ + 20 mV, then levelled off at positive potentials. The normalized I_{hERG} tail I-V relation exhibited a left-ward voltage-shift in the presence of phenanthrene. In control solution the $V_{0.5}$ value obtained was 1.3 ± 1.6 mV (k = 7.2 ± 0.2 mV, n = 16), whilst in 10 μM phenanthrene $V_{0.5}$ was − 8.9 ± 1.5 mV ($P < 0.001$ vs Control; k unchanged 7.8 ± 0.3 mV, n = 16). Thus, phenanthrene produced a ~ 10 mV negative shift in voltage-dependent activation, which accounts for the apparent increase in I_{hERG} at negative voltages. This phenomenon has been observed previously for other hERG-blocking agents including azimilide [40], 4-aminopyridine [41], sarizotan [35]. The steep change in fractional inhibition coincided with the steep portion of the voltage-dependent activation relation for I_{hERG}, consistent with an activation-dependent inhibitory mechanism.

Depolarization time and I_{hERG} inhibition by phenanthrene

The voltage-dependence of I_{hERG} inhibition by phenanthrene indicates gating dependence of channel inhibition by the compound. To probe this further, we conducted experiments in which the extent of I_{hERG} inhibition by short and longer duration pulses was compared [42;43]. For these experiments, activating pulses to + 20 mV of different durations were applied: 100 ms and 800 ms. These were first applied in control superfusate, the cell under study was then rested for 3–5 minutes whilst being superfused with 10 μM phenanthrene and the protocol was reapplied. The extent of I_{hERG} inhibition by the compound at the shorter and longer duration commands was then evaluated by assessing extent of tail current block. As shown in Fig. 4Ai, for the 100 ms duration command the tail current in the presence of phenanthrene was actually larger than that in control. This is likely a consequence of the facilitated activation evident in the I-V experiments described in Fig. 3. As channels would have been closed prior to application of this test pulse, the result indicates either that 100 ms was sufficient for the compound to interact with the channel once channel gating was initiated, or that phenanthrene was able to gain access when the channel was closed. With the longer duration voltage command, shown in Fig. 4Aii, it is clear that substantial I_{hERG} inhibition occurred. Mean fractional block data are plotted in Fig. 4B, showing a clear statistically significant difference between the compound effects on tail current amplitude for 100 and 800 ms pulse durations ($P < 0.01$; $n = 5$). Thus, there was clear dependence of the response to phenanthrene on the duration of the activating test command. A monoexponential fit to tail currents elicited by different duration commands to + 20 mV between 100 and 800 ms (not shown) suggested that activation was incomplete at 800 ms in control but not phenanthrene containing solution, with estimated τ_{act} values of 341 ± 30 ms and 205 ± 37 ms, respectively ($p < 0.05$). Thus, phenanthrene accelerated the time-course of I_{hERG} activation.

Probing the mechanism of I_{hERG} inhibition with mutagenesis

In order to investigate gating-dependence of inhibition further, experiments were conducted using the N588K attenuatedinactivation mutation. The N588 residue is located in the external S5-Pore linker region of the channel; it has utility for investigating inactivation dependence of hERG inhibition [44;45] as it perturbs inactivation gating without directly modifying channel structure within regions of the pore typically implicated in drug binding. Figure 5Ai shows the effect of 30 μM phenanthrene on WT I_{hERG}, illustrating marked current inhibition by this concentration of the compound. By contrast, only slight inhibition of N588K I_{hERG} was observed (Fig. 5Aii, mean data in Fig. 5H). This indicates that inactivation competency was required for optimal interaction between phenanthrene and its binding site on the hERG channel. The S624 residue, located near the base of the hERG channel selectivity filter, has been implicated in I_{hERG} inhibition by a number of compounds (e.g. [46;47]. Figure 5B shows effects of 30 μM phenanthrene on S624A I_{hERG}. Pulse-current appeared significantly augmented and tail current amplitude unchanged by phenanthrene with the S624A mutation (mean data are shown in Fig. 5H). This implicates the S624 residue, directly or indirectly, as being important for phenanthrene binding to the hERG channel. We proceeded to investigate the roles of two aromatic residues, Y652 and F656 in phenanthrene action. For virtually all compounds that have been investigated in detail, interactions with one or both of these residues are obligatory for drug binding and channel inhibition [17;48]. Remarkably, the inhibitory effect

of 30 μM phenanthrene on Y652A I_{hERG} (Fig. 5C, mean data in Fig. 5H) was significantly greater than on WT I_{hERG}. Supplemental Fig. 3A shows mean concentration-response data for Y652A I_{hERG}, which yielded an IC_{50} of 4.35 ± 1.26 μM, Hill slope: 0.54 ± 0.16. The F656V mutation (Fig. 5D, mean data in Fig. 5H) also did not impair the inhibitory effect of phenanthrene, showing a trend towards increased block, albeit that this was statistically insignificant. We also investigated effects of a second mutation at F656: F656T. A small reduction of inhibition of F656T I_{hERG} by 30 μM is shown in the exemplar traces shown in Fig. 5E; however, mean pooled data (Fig. 5H) show that this effect was not statistically significantly different from block of WT I_{hERG}. Phenanthrene is therefore distinct from most hERG-blocking drugs thus far studied in not requiring aromatic residues at positions 652 and 656 for inhibition to occur. Residue Y652 has previously been implicated in voltage-dependence of I_{hERG} inhibition (e.g. [49;50]. In this respect, it is notable that whilst the Y652A mutation increased rather than decreased phenanthrene inhibition, it largely abolished the voltage-dependence of inhibition seen for WT I_{hERG} (Supplemental Fig. 3B).

Residue F557 on the S5 helix of the hERG channel has been identified as a determinant of I_{hERG} inhibition and lies adjacent to Y652 on the S6 helix [29;51–53]. No inhibition of F557L I_{hERG} was observed with 3 concentrations of phenanthrene (between 10 and 100 μM). Figure 5F shows representative traces of effects of 30 μM phenanthrene on F557L I_{hERG}. No inhibition was evident, rather the pulse and peak tail current were slightly larger in the presence of phenanthrene than in control solution (mean data shown in Fig. 5H). This observation implicates residue F557 as of critical importance to phenanthrene inhibition of I_{hERG}. The publication of a cryo-EM structure for hERG has shown the presence of 4 hydrophobic pockets that surround the central cavity of the channel, which may provide interaction site(s) for drugs [33]. Lipophilic drug access to the channel pore involving F557 and S6 residue M651 has recently been suggested for the bradycardic agent ivabradine [52]. Figure 5G shows effects of the M651A mutation on I_{hERG} block by 30 μM phenanthrene. In contrast to WT I_{hERG} M651A was little affected by phenanthrene (mean data shown in Fig. 5H), implicating this residue in the compound's inhibitory action.

Phenanthrene inhibition explored through computational docking

Low energy score docking poses consistent with mutagenesis data were not obtained for phenanthrene bound into the structure of hERG obtained from cryo electron microscopy (cryo-EM). Phenanthrene was unable to make multiple interactions with aromatic side chains when docked into the canonical pore blocker site below the selectivity filter within the K + permeation path (not shown). This results from the absence of F656 side chain conformations in the cryo-EM structure that project the side chains towards the pore and the rigidity of the phenanthrene tri-aromatic ring structure that limits its ability to conform to the arrangement of Y656 side chains within the pore. The rigidity of the structure also limited identification of low energy score configurations for phenanthrene binding within one of the hydrophobic pockets below the pore helix in the cryo-EM structure. In addition, the projection of the F656 side chains towards the S5 helix in the cryo-EM structure limits the localisation of phenanthrene in a configuration that allows interactions with the side chains of F557 and M651.

Low energy poses were obtained for phenanthrene bound within a side pocket of a hERG model obtained by very short MD simulation in which an F656 side chain rotated away from its configuration in the cryo-EM structure towards the pore. A low energy score pose consistent with the mutagenesis data is shown in Fig. 6. Phenanthrene sits deep within a hydrophobic pocket making aromatic stacking interactions with F557 and hydrophobic interactions with M651. This binding mode is facilitated by the rotation of the F656 side chain out of this binding pocket.

Discussion

Potency of observed I_{hERG} inhibition and environmental relevance for human health

Phenanthrene has previously been reported to inhibit native I_{Kr} from bluefin tuna myocytes at room temperature by nearly 60% at 5 µM and by over 80% at 25 µM [11]. 30 µM phenanthrene inhibited rainbow trout myocyte I_{Kr} by 79% [13], whilst an IC_{50} for inhibition of brown trout myocyte I_{Kr} of 7.2 µM has been reported [14]. Very recent work has indicated that I_{Kr} from zebrafish ventricular myocytes is inhibited by phenanthrene with an IC_{50} of 3.3 µM [15], which is in fair agreement with the value of 8.7 µM obtained in this study for I_{zERG}. We observed IC_{50} values for I_{hERG} carried by hERG1a channels of 16.8 µM and for co-expressed hERG1a/1b of 1.7 µM, which are broadly comparable to the potency of phenanthrene against fish I_{Kr}.

Data on plasma levels of PAHs in humans are sparse, in part because convention focuses on other measures – either PAH concentrations per given volume of air, or urinary metabolite concentrations. Plasma concentrations of phenanthrene and/or other PAHs in the nM range have been reported in the literature (e.g. [54;55]. However, as has been highlighted elsewhere, phenanthrene is highly lipophilic and so is likely to exhibit tissue accumulation [1]. This has been demonstrated for waterborne exposures of developing fish embryos in which phenanthrene tissue levels typically reach the low micromolar range (e.g., [56] and in similarly substantial accumulations of PAHs in avian tissues [57]. Road pavers and coke plant workers show urinary phenanthrol levels of ~ 35 µg/L to 686 µg/L (approximately 0.2–3.5 µM; [58]. Such data are suggestive of quite high concentrations in subpopulations who, through occupational risk, are exposed routinely to high levels of PAHs. Moreover, a recent comparison of serum phenanthrene levels in Greek citizens found increased levels in those with heart failure (231 µg/L; ~1.3 µM) compared to those without heart failure (56.5 µg/L; 314 nM) [59]. Thus, it is likely to be those with high PAH exposure and/or those with pre-existing cardiovascular morbidity who will be most susceptible to adverse reactions to phenanthrene.

Mechanism of block

Phenanthrene has a simple structure of three fused benzene rings and given its high lipophilicity [1], a natural question is whether it exerts direct interactions with the hERG channel or whether its inhibitory effect is secondary to accumulation of phenanthrene in membrane lipid? Multiple lines of evidence provided here support a direct interaction with the channel. First, the lack of significant effect of

phenanthrene on hERG trafficking at 3 and 30 μM (Supplementary Fig. 1), indicates that altered trafficking is unlikely to contribute an additional inhibitory effect on the channel's function during chronic exposure. Second, the structurally related antimalarial drug halofantrine (3-(dibutylamino)-1-[1,3-dichloro-6-(trifluoromethyl)phenanthren-9-yl]propan-1-ol), which contains a substituted phenanthrene, is known to inhibit I_{hERG} in an open state-dependent fashion, with sensitivity to mutation of S6 helical aromatic residues [60;61]. Third, in this study phenanthrene inhibition of WT I_{hERG} exhibited voltage- and time-dependence that demonstrate contingency on channel gating for the compound to access its inhibitory binding site. Fourth, the profound reduction in the I_{hERG} inhibitory effect of phenanthrene on inactivation-impaired N588K channels indicates a requirement for intact inactivation gating for optimal access to the inhibitory binding site. Finally, the results of our mutagenesis experiments and docking simulations implicate specific mutations as phenanthrene binding determinants. Thus, the results of this study support a conclusion that phenanthrene acts as a direct hERG channel inhibitor. To our knowledge, the data from this study constitute the most detailed information on the basis of phenanthrene inhibition of any ion channel or electrogenic transporter.

The acceleration of WT $I_{hERG(1a)}$ and I_{zERG} deactivation seen here by phenanthrene is unusual, although it is in agreement with recent observations on the effect of phenanthrene on zebrafish native I_{Kr} [62]. Acceleration of I_{hERG} deactivation precludes a "foot-in-door" inhibitory mechanism in which a compound's presence in the inner cavity slows closure of the activation gate. The relationship between deactivation acceleration by phenanthrene and the compound's ability to block the channel appears complex: both N588K and S624A I_{hERG}, which were largely resistant to phenanthrene inhibition, showed little or no effect of the compound on deactivation parameters (Supplemental Fig. 4), consistent with a link between current blocking and deactivation accelerating actions. On the other hand, F557L current was augmented not inhibited by phenanthrene and yet exhibited faster deactivation than in control (Fig. 5 and online supplement text), consistent with independence between current blocking and deactivation accelerating actions. It is not straightforward to unify these observations, though the F557L result indicates that deactivation acceleration is not inextricably linked to channel block by phenanthrene. There was, however, a strong correlation between the current's deactivation rate in *control* solution and the derived IC_{50} for phenanthrene inhibition (shown by plotting IC_{50} against fast and slow inactivation τ for hERG 1a, hERG1a/b and zERG; see Supplemental Fig. 5). hERG1b is identical to hERG1a except for its abbreviated N terminus, which lacks the EAG domain that is known to be important for slow deactivation (Supplemental Fig. 5 and [63]. The faster deactivation of $I_{hERG1a/1b}$ in control conditions was not further accelerated by phenanthrene, suggesting that a full complement of intact N-termini was not required for phenanthrene to inhibit hERG channels. However, it seems likely that conformational changes associated with fast deactivation may be involved in optimising the compound's interaction with or access to binding residues in the pore.

Perhaps the most surprising results of this study are those pertaining to the likely interaction site through which phenanthrene inhibits I_{hERG}. Virtually all compounds that have been hitherto investigated have shown a strong dependence on interactions with one or both of S6 Y652 and F656: mutations of these

residues typically reduce inhibitory potency [18;48]. Indeed, structurally related halofantrine conforms to this observation [61]. By contrast, for phenanthrene, mutations at F656 failed significantly to reduce I_{hERG} inhibition and the Y652A mutation increased blocking potency. To our knowledge there is only one prior report of a compound for which Y652A increases inhibitory potency: capsaicin [64]. In that study, the IC_{50} for capsaicin was 4-fold lower for Y652A than for WT I_{hERG} and the F656A mutation did not alter potency [64]. Obligatory determinants of capsaicin binding were not identified [64]. There is little structural similarity between capsaicin and phenanthrene and binding determinants are unlikely to be similar for the two compounds. The recent cryo-EM structure of hERG contains hydrophobic pockets surrounding the central cavity that are large enough to accommodate drug molecules [33]. F557 on the S5 helix lies deep within the pockets and has been implicated in the binding of a number of drugs [29;35;51;65]. Recent work has implicated both F557 and M561 in hERG block by the bradycardic agent ivabradine, with mutation of M651 influencing state-dependent dynamics of aromatic residue cassettes at the pore-lipid interface [65]. These observations are consistent with recent identification with other K^+ channels that hydrophobic pockets can provide inhibitor binding sites away from the K^+ permeation path [66–68].

Docking of phenanthrene identifies a site within the side pockets that can accommodate phenanthrene in structures in which the F656 side chain is rotated towards the pore. In other words, the reconfiguration of F656 into a pore-facing orientation creates space for phenanthrene to bind into a site in which interactions with F557 and M651 side chains are made (Fig. 6), consistent with our mutagenesis results (Fig. 5). Recent simulations starting with the cryo-EM structure have indicated that rotation of the F656 side chain towards the pore occurs readily and is required for optimal matching of computational analysis of drug binding with experimental mutagenesis data [29;65;69;70], although in a recent bound structure for astemizole, direct interactions of the drug with F656 made only a minor contribution to overall binding [71]. Our results suggest that rotation of F656 side chains towards the pore may be required both for binding of some classical pore blockers (to maximise pore blocker interactions with aromatic side chains within the pore) and for inhibitors that bind deep within hERG pore domain side pockets (to free space for inhibitor binding). In any case, binding modes that accommodate phenanthrene deep within a pocket on the S5-S6 interface (Fig. 6) are also consistent with a minimal effect of F656 mutants on phenanthrene block (Fig. 5), in contrast with a general requirement for F656 as a binding determinant for positively charged pore blockers [48]. The location of the binding site away from the K^+ permeation path below the selectivity filter is also consistent with the absence of effect of inward K^+ current which can suffice to attenuate the effects of blockers that bind within the K^+ permeation path [72;73].

The enhancement of phenanthrene block in the Y652A mutant is less readily explained by the docking analysis although the absence of a requirement for Y652 interactions is consistent with the location for phenanthrene identified by docking guided by mutagenesis (Fig. 6). The voltage-dependence of phenanthrene block is associated with a voltage-dependent reorientation of the Y652 side chain [29;74], implicating a change on the configuration of the Y652 side chain in promoting block. One possibility is that voltage dependent reorientation of the Y652 side chain towards the bottom of the selectivity filter in

response to membrane depolarization promotes hydrogen bonding between the tyrosine phenolic hydroxyl group and the S624 side chain hydroxyl group and this facilitates phenanthrene access to the binding pocket. Such an effect might explain the attenuation of phenanthrene block in the S624A mutant.

The Hill coefficients for the concentration response data for phenanthrene block of WT I_{hERG} (Figs. 1 and 2) are consistent with a lack of cooperativity which, taken together with the small size of phenanthrene, suggests that binding to a single hERG pore subunit is sufficient for channel block to occur. Although hydrophobic pocket binding has been identified for several K^+ channel inhibitors [66–68], the mechanism by which this leads to channel inhibition remains unclear. One possibility is that inhibition involves perturbation of the selectivity filter. A curious observation is that some hERG activators which act by attenuating inactivation also bind within hERG pockets and so there may be subtle differences in blocker and activator binding that affect structure around the selectivity filter with opposite effects. Consistent with this idea a recent study on hERG activators that are likely to bind within pockets has shown that subtle chemical modification of activators can turn them into blockers [75].

In conclusion, this study demonstrates that the ubiquitous hydrocarbon pollutant phenanthrene produces an acute pharmacological block of the hERG potassium channel at concentrations compatible with tissue accumulation. We have also identified phenanthrene as a direct channel inhibitor that is mechanistically distinct from canonical hERG blockers, suggesting a broader sensitivity of this channel to adverse chemical impact than simply an off-target sensitivity to pharmaceuticals. Importantly, whilst candidate pharmaceuticals with hERG-blocking activity can be withdrawn from development, this is not the case for phenanthrene – a pervasive pollutant in air and water. As I_{Kr} is critical for human ventricular repolarization, further work is warranted to determine consequences of this effect for human ventricular electrophysiology and arrhythmia risk, and whether tricyclic pollutants contribute to the morbidity and mortality associated with urban air pollution.

Declarations

Funding:

This work was funded by the British Heart Foundation: PG/17/77/33125, PG/17/89/33414, PG/20/10252, FS/19/44/34424, PG /19/26/34302

Conflicts of interest/competing interests:

The authors declare that they have no actual or potential competing interests.

Availability of data and material:

Data for the study are included in the manuscript and supplementary information. Materials for the study will be made available on reasonable request.

Code availability:

The cryo-EM structure used for this study is available at the RCSB Protein Data Bank, PDB code: 5VA2

Authors contributions:

JCH and HAS conceived the study. JCH, EAM, CED, SCH designed the study. JCH, HAS, CED and SCH obtained research funding and provided supervision. Material preparation, data collection and analysis were performed by EAM, OH, YZ, CED. The first draft of the manuscript was written by JCH, EAM, CED, SCH, OH. All authors reviewed/commented on manuscript drafts prior to submission. All authors read and approved the final manuscript.

Acknowledgements: The authors thank the British Heart Foundation for funding (PG/17/77/33125, PG/17/89/33414, PG/20/10252, FS/19/44/34424, PG /19/26/34302) and Dr John Incardona for helpful discussion and comments on the manuscript.

References

1. Marris CR, Kompella SN, Miller MR, Incardona JP, Brette F, Hancox JC, Sorhus E, Shiels HA (2020) Polyaromatic hydrocarbons in pollution: a heart-breaking matter. J Physiol 598:227–247
2. Phillips DH (1983) Fifty years of benzo(a)pyrene. Nature 303:468–472
3. Pampanin DM, Sydnes MO (2013) Polycyclic aromatic hydrocarbons a constituent of petroleum: presence and influence in the aquatic environment. In Kutcherov, V and Kolesnikov, A. Hydrocarbon, 84–118. 2013 Intech Open
4. Benner BA, Gordon GE, Wise SA (1989) Mobile sources of atmospheric polycyclic aromatic-hydrocarbons - a roadway tunnel study. EnvironSciTechnol 23:1269–1278
5. Li Z, Porter EN, Sjodin A, Needham LL, Lee S, Russell AG, Mulholland JA. Characterization of PM2.5-bound polycyclic aromatic hydrocarbons in Atlanta—Seasonal variations at urban, suburban, and rural ambient air monitoring sites. Atmospheric Environment 43: 4187–4193
6. Rogge WF, Ondov JM, Bernardo-Bricker A, Sevimoglu O (2011) Baltimore PM2.5 Supersite: highly time-resolved organic compounds–sampling duration and phase distribution–implications for health effects studies. Anal Bioanal Chem 401:3069–3082
7. Tsapakis M, Stephanou EG (2005) Occurrence of gaseous and particulate polycyclic aromatic hydrocarbons in the urban atmosphere: study of sources and ambient temperature effect on the gas/particle concentration and distribution. Environ Pollut 133:147–156
8. Incardona JP, Scholz NL, Case Study: The 2010 Deepwater Horizon Oil Spill and Its Environmental Developmental Impacts. In Burggren, W and Dubansky, B. Development and Environment, 235–283 (2018) Springer International Publisher AG
9. Incardona JP, Collier TK, Scholz NL (2004) Defects in cardiac function precede morphological abnormalities in fish embryos exposed to polycyclic aromatic hydrocarbons. Toxicol Appl Pharmacol 196:191–205

10. Incardona JP, Gardner LD, Linbo TL, Brown TL, Esbaugh AJ, Mager EM, Stieglitz JD, French BL, Labenia JS, Laetz CA, Tagal M, Sloan CA, Elizur A, Benetti DD, Grosell M, Block BA, Scholz NL (2014) Deepwater Horizon crude oil impacts the developing hearts of large predatory pelagic fish. Proc Natl Acad Sci U S A 111:E1510–E1518
11. Brette F, Machado B, Cros C, Incardona JP, Scholz NL, Block BA (2014) Crude oil impairs cardiac excitation-contraction coupling in fish. Science 343:772–776
12. Brette F, Shiels HA, Galli GL, Cros C, Incardona JP, Scholz NL, Block BA (2017) A Novel Cardiotoxic Mechanism for a Pervasive Global Pollutant. Sci Rep 7:41476
13. Vehniainen ER, Haverinen J, Vornanen M (2019) Polycyclic Aromatic Hydrocarbons Phenanthrene and Retene Modify the Action Potential via Multiple Ion Currents in Rainbow Trout (Oncorhynchus mykiss) Cardiac Myocytes. Environ Toxicol Chem 38:2145–2153
14. Ainerua MO, Tinwell J, Kompella SN, Sorhus E, White KN, van Dongen BE, Shiels HA (2020) Understanding the cardiac toxicity of the anthropogenic pollutant phenanthrene on the freshwater indicator species, the brown trout (Salmo trutta): From whole heart to cardiomyocytes. Chemosphere 239:124608
15. Kompella SN, Brette F, Hancox JC, Shiels HA (2021) Phenanthrene impacts zebrafish cardiomyocyte excitability by inhibiting I_{Kr} and shortening action potential duration. J Gen Physiol 153:e202012733
16. Meador JP, Nahrgang J (2019) Characterizing Crude Oil Toxicity to Early-Life Stage Fish Based On a Complex Mixture: Are We Making Unsupported Assumptions? Environ Sci Technol 53:11080–11092
17. Sanguinetti MC, Tristani-Firouzi M (2006) hERG potassium channels and cardiac arrhythmia. Nature 440:463–469
18. Hancox JC, McPate MJ, El Harchi A, Zhang YH (2008) The hERG potassium channel and hERG screening for drug-induced torsades de pointes. Pharmacol Ther 119:118–132
19. Sanguinetti MC, Jiang C, Curran ME, Keating MT (1995) A mechanistic link between an inherited and an acquired cardiac arrhythmia: HERG encodes the I_{Kr} potassium channel. Cell 81:299–307
20. Trudeau MC, Warmke JW, Ganetzky B, Robertson GA (1995) HERG, an inward rectifier in the voltage-gated potassium channel family. Science 269:92–95
21. Hancox JC, Whittaker DG, Du C, Stuart AG, Zhang H (2018) Emerging therapeutic targets in the short QT syndrome. Expert Opin Ther Targets 22:439–451
22. Al Moubarak E, Shiels HA, Zhang Y, Du C, Dempsey CE, Hancox JC Inhibition of hERG Potassium Channels by the Polycylic Aromatic Hydrocarbon, Phenanthrene (2020) Biophys J 118:109a
23. Al Moubarak E, Shiels H, Zhang Y, Dempsey CE, Hancox JC (2019) Poster Communications: Inhibition of the human Ether-à-go-go-Related Gene (hERG) potassium channels by phenanthrene. Proc Physiol Soc 43:PC016
24. Du C, Zhang Y, El HA, Dempsey CE, Hancox JC (2014) Ranolazine inhibition of hERG potassium channels: Drug-pore interactions and reduced potency against inactivation mutants. J Mol Cell Cardiol 74C:220–230

25. Melgari D, Brack KE, Zhang C, Zhang Y, El Harchi A, Mitcheson JS, Dempsey CE, Ng GA, Hancox JC (2015) hERG potassium channel blockade by the HCN channel inhibitor bradycardic agent ivabradine. J Am Heart Assoc 4:e001813
26. Zhang Y, Colenso CK, El Harchi A, Cheng H, Witchel HJ, Dempsey CE, Hancox JC (2016) Interactions between amiodarone and the hERG potassium channel pore determined with mutagenesis and in silico docking. Biochem Pharmacol 113:24–35
27. Zhou Z, Gong Q, Ye B, Fan Z, Makielski JC, Robertson GA, January CT (1998) Properties of HERG channels stably expressed in HEK 293 cells studied at physiological temperature. Biophys J 74:230–241
28. McPate MJ, Duncan RS, Milnes JT, Witchel HJ, Hancox JC (2005) The N588K-HERG K + channel mutation in the 'short QT syndrome': mechanism of gain-in-function determined at 37^{o}C. Biochem Biophys Res Comm 334:441–449
29. Helliwell MV, Zhang Y, El Harchi A, Du C, Hancox JC, Dempsey CE (2018) Structural implications of hERG K^+ channel block by a high affinity minimally-structured blocker. J Biol Chem 293:7040–7057
30. Du CY, El Harchi A, McPate MJ, Orchard CH, Hancox JC (2011) Enhanced inhibitory effect of acidosis on hERG potassium channels that incorporate the hERG1b isoform. Biochem Biophys Res Commun 405:222–227
31. El Harchi A, Butler AS, Zhang Y, Dempsey CE, Hancox JC (2020) The macrolide drug erythromycin does not protect the hERG channel from inhibition by thioridazine and terfenadine. Physiol Rep 8:e14385
32. Al Moubarak E, Zhang Y, Dempsey CE, Zhang H, Harmer SC, Hancox JC (2020) Serine mutation of a conserved threonine in the hERG K^+ channel S6-pore region leads to loss-of-function through trafficking impairment. Biochem Biophys Res Comm 526:1085–1091
33. Wang W, MacKinnon R (2017) Cryo-EM Structure of the Open Human Ether-a-go-go-Related K + Channel hERG. Cell 169:422–430
34. Dempsey CE, Wright D, Colenso CK, Sessions RB, Hancox JC (2014) Assessing HERG pore models as templates for drug docking using published experimental constraints: the inactivated state in the context of drug block. J Chem Inf Model 54:601–612
35. Cheng H, Du C, Zhang Y, James AF, Dempsey CE, Abdala AP, Hancox JC (2019) Potent hERG channel inhibition by sarizotan, an investigative treatment for Rett Syndrome. J Mol Cell Cardiol 135:22–30
36. Wible BA, Hawryluk P, Ficker E, Kuryshev YA, Kirsch G, Brown AM (2005) HERG-Lite: a novel comprehensive high-throughput screen for drug-induced hERG risk. J Pharmacol Toxicol Methods 52:136–145
37. Jones DK, Liu F, Vaidyanathan R, Eckhardt LL, Trudeau MC, Robertson GA (2014) hERG 1b is critical for human cardiac repolarization. Proc Natl Acad Sci U S A 111:18073–18077
38. Jones EM, Roti Roti EC, Wang J, Robertson GA (2004) Cardiac I_{Kr} channels minimally comprise hERG 1a and 1b subunits. J Biol Chem 279:44690–44694

39. Sale H, Wang J, O'Hara TJ, Tester DJ, Phartiyal P, He JQ, Rudy Y, Ackerman MJ, Robertson GA (2008) Physiological properties of hERG 1a/1b heteromeric currents and a hERG 1b-specific mutation associated with Long-QT syndrome. Circ Res 103:e81–e95
40. Jiang M, Dun W, Fan JS, Tseng GN (1999) Use-dependent 'agonist' effect of azimilide on the HERG channel. J Pharmacol Exp Ther 291:1324–1336
41. Ridley JM, Milnes JT, Zhang YH, Witchel HJ, Hancox JC (2003) Inhibition of HERG K + current and prolongation of the guinea-pig ventricular action potential by 4-aminopyridine. J Physiol 549:667–672
42. Milnes JT, Crociani O, Arcangeli A, Hancox JC, Witchel HJ (2003) Blockade of HERG potassium currents by fluvoxamine: incomplete attenuation by S6 mutations at F656 or Y652. Br J Pharmacol 139:887–898
43. Duncan RS, Ridley JM, Dempsey CE, Leishman DJ, Leaney JL, Hancox JC, Witchel HJ (2006) Erythromycin block of the HERG K^+ channel: accessibility to F656 and Y652. Biochem Biophys Res Comm 341:500–506
44. McPate MJ, Duncan RS, Hancox JC, Witchel HJ (2008) Pharmacology of the short QT syndrome N588K-hERG K^+ channel mutation: differential impact on selected class I and class III antiarrhythmic drugs. Br J Pharmacol 155:957–966
45. Perrin MJ, Kuchel PW, Campbell TJ, Vandenberg JI (2008) Drug binding to the inactivated state is necessary but not sufficient for high-affinity binding to human ether-à-go-go-related gene channels. Mol Pharmacol 74:1443–1452
46. Mitcheson JS, Chen J, Lin M, Culberson C, Sanguinetti MC (2000) A structural basis for drug-induced long QT syndrome. Proc Natl Acad Sci U S A 97:12329–12333
47. Perry M, Stansfeld PJ, Leaney J, Wood C, de Groot MJ, Leishman D, Sutcliffe MJ, Mitcheson JS (2006) Drug binding interactions in the inner cavity of HERG channels: molecular insights from structure-activity relationships of clofilium and ibutilide analogs. Mol Pharmacol 69:509–519
48. Butler A, Helliwell MV, Zhang Y, Hancox JC, Dempsey CE (2019) An Update on the Structure of hERG. Front Pharmacol 10:1572
49. Sanchez-Chapula JA, Ferrer T, Navarro-Polanco RA, Sanguinetti MC (2003) Voltage-dependent profile of human ether-a-go-go-related gene channel block is influenced by a single residue in the S6 transmembrane domain. Mol Pharmacol 63:1051–1058
50. Alexandrou AJ, Duncan RS, Sullivan A, Hancox JC, Leishman DJ, Witchel HJ, Leaney JL (2006) Mechanism of hERG K^+ channel blockade by the fluoroquinolone antibiotic moxifloxacin. Br J Pharmacol 147:905–916
51. Saxena P, Zangerl-Plessl EM, Linder T, Windisch A, Hohaus A, Timin E, Hering S, Stary-Weinzinger A (2016) New potential binding determinant for hERG channel inhibitors. Sci Rep 6:24182
52. Duff HJ, Noskov SY, Muruve D, Perlovic G, Ol KM, Sharapova A, Gerull B, Guo J, Kudaibergenova M, Perissinotti L (2019) The Pore-Lipid Interface: Role of Amino Acid Determinants of Lipophilic Access

by Ivabradine to the hERG1 Pore Domain. Mol Pharmacol 92:259–271

53. Butler A, Helliwell MV, Zhang Y, Hancox JC, Dempsey CE (2019) An Update on the Structure of hERG. Front Pharmacol 10:1572
54. Zhong Y, Wang J, Carmella SG, Hochalter JB, Rauch D, Oliver A, Jensen J, Hatsukami DK, Upadhyaya P, Zimmerman C, Hecht SS (2011) Metabolism of [D10]phenanthrene to tetraols in smokers for potential lung cancer susceptibility assessment: comparison of oral and inhalation routes of administration. J Pharmacol Exp Ther 338:353–361
55. Camacho M, Boada LD, Oros J, Calabuig P, Zumbado M, Luzardo OP (2012) Comparative study of polycyclic aromatic hydrocarbons (PAHs) in plasma of Eastern Atlantic juvenile and adult nesting loggerhead sea turtles (Caretta caretta). Mar Pollut Bull 64:1974–1980
56. Incardona JP, Carls MG, Day HL, Sloan CA, Bolton JL, Collier TK, Scholz NL (2009) Cardiac arrhythmia is the primary response of embryonic Pacific herring (Clupea pallasi) exposed to crude oil during weathering. Environ Sci Technol 43:201–207
57. Dhananjayan V, Muralidharan S (2013) Levels of polycyclic aromatic hydrocarbons, polychlorinated biphenyls, and organochlorine pesticides in various tissues of white-backed vulture in India. Biomed Res Int 2013: 190353
58. Jacob J, Seidel A (2002) Biomonitoring of polycyclic aromatic hydrocarbons in human urine. J Chromatogr B Analyt Technol Biomed Life Sci 778:31–47
59. Chrysochou E, Kanellopoulos PG, Koukoulakis KG, Sakellari A, Karavoltsos S, Minaidis M, Bakeas E (2021) Heart Failure and PAHs, OHPAHs, and Trace Elements Levels in Human Serum: Results from a Preliminary Pilot Study in Greek Population and the Possible Impact of Air Pollution. Molecules 26:3207
60. Mbai M, Rajamani S, January CT (2002) The anti-malarial drug halofantrine and its metabolite N-desbutylhalofantrine block HERG potassium channels. Cardiovasc Res 55:799–805
61. Sanchez-Chapula JA, Navarro-Polanco RA, Sanguinetti MC (2004) Block of wild-type and inactivation-deficient human ether-a-go-go-related gene K^+ channels by halofantrine. Naunyn Schmiedebergs Arch Pharmacol 370:484–491
62. Kompella SN, Hancox JC, Brette F, Shiels H (2020) Small heart revealing big insights: understanding pharmacology of cardiotoxic air pollutant phenanthrene using zebrafish. Future Physiology 2020, OC14. 2020
63. Muskett FW, Thouta S, Thomson SJ, Bowen A, Stansfeld PJ, Mitcheson JS (2011) Mechanistic insight into human ether-a-go-go-related gene (hERG) K^+ channel deactivation gating from the solution structure of the EAG domain. J Biol Chem 286:6184–6191
64. Xing J, Ma J, Zhang P, Fan X (2010) Block effect of capsaicin on hERG potassium currents is enhanced by S6 mutation at Y652. Eur J Pharmacol 630:1–9
65. Perissinotti L, Guo J, Kudaibergenova M, Lees-Miller J, Ol'khovich M, Sharapova A, Perlovich GL, Muruve DA, Gerull B, Noskov SY, Duff HJ (2019) The Pore-Lipid Interface: Role of Amino-Acid

Determinants of Lipophilic Access by Ivabradine to the hERG1 Pore Domain. Mol Pharmacol 96:259–271

66. Marzian S, Stansfeld PJ, Rapedius M, Rinne S, Nematian-Ardestani E, Abbruzzese JL, Steinmeyer K, Sansom MS, Sanguinetti MC, Baukrowitz T, Decher N (2013) Side pockets provide the basis for a new mechanism of Kv channel-specific inhibition. Nat Chem Biol 9:507–513
67. Dong YY, Pike AC, Mackenzie A, McClenaghan C, Aryal P, Dong L, Quigley A, Grieben M, Goubin S, Mukhopadhyay S, Ruda GF, Clausen MV, Cao L, Brennan PE, Burgess-Brown NA, Sansom MS, Tucker SJ, Carpenter EP (2015) K2P channel gating mechanisms revealed by structures of TREK-2 and a complex with Prozac. Science 347:1256–1259
68. Wrobel E, Rothenberg I, Krisp C, Hundt F, Fraenzel B, Eckey K, Linders JT, Gallacher DJ, Towart R, Pott L, Pusch M, Yang T, Roden DM, Kurata HT, Schulze-Bahr E, Strutz-Seebohm N, Wolters D, Seebohm G (2016) KCNE1 induces fenestration in the Kv7.1/KCNE1 channel complex that allows for highly specific pharmacological targeting. Nat Commun 7:12795
69. Negami T, Araki M, Okuno Y, Terada T (2019) Calculation of absolute binding free energies between the hERG channel and structurally diverse drugs. Sci Rep 9:16586
70. Dickson CJ, Velez-Vega C, Duca JS (2020) Revealing Molecular Determinants of hERG Blocker and Activator Binding. J Chem Inf Model 60:192–203
71. Asai T, Adachi N, Moriya T, Oki H, Maru T, Kawasaki M, Suzuki K, Chen S, Ishii R, Yonemori K, Igaki S, Yasuda S, Ogasawara S, Senda T, Murata T (2020) Cryo-EM structure of K^+-bound hERG channel complexed with the blocker astemizole. Structure 29:203–212
72. Wang S, Morales MJ, Liu S, Strauss HC, Rasmusson RL (1997) Modulation of HERG affinity for E-4031 by $[K]_o$ and C-type inactivation. FEBS Lett 417:43–47
73. Ridley JM, Milnes JT, Witchel HJ, Hancox JC (2004) High affinity HERG K^+ channel blockade by the antiarrhythmic agent dronedarone: resistance to mutations of the S6 residues Y652 and F656. Biochem Biophys Res Comm 325:883–891
74. Barchad-Avitzur O, Priest MF, Dekel N, Bezanilla F, Parnas H, Ben-Chaim Y (2016) A Novel Voltage Sensor in the Orthosteric Binding Site of the M2 Muscarinic Receptor. Biophys J 111:1396–1408
75. van Veldhoven JPD, Campostrini G, van Gessel CJE, Ward-van OD, Liu R, Mummery CL, Bellin M, IJzerman AP (2020) Targeting the Kv11.1 (hERG) channel with allosteric modulators. Synthesis and biological evaluation of three novel series of LUF7346 derivatives. Eur J Med Chem 212:113033

Figures

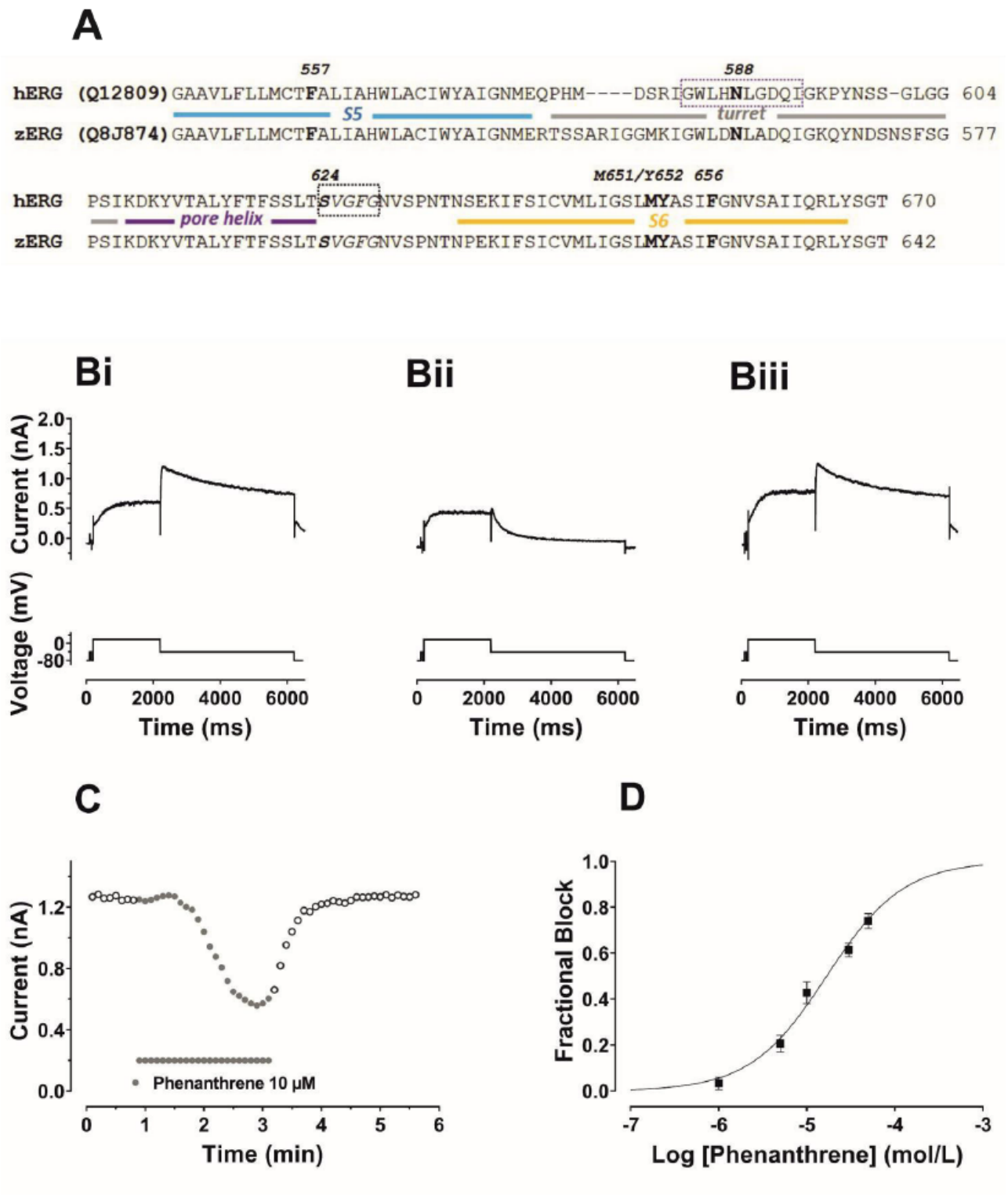

Figure 1

A: Sequence alignments of zERG and hERG showing very high homology in the pore helix, S5 and S6 regions that contribute to the canonical drug binding site and residues investigated here for phenanthrene. The structural elements of the channel pore domain are coloured to match the structural figure in Figure 6a. B: Upper traces show Bi: Control IhERG, Bii: IhERG during application of 10 µM phenanthrene (Phen), Biii: Current during washout of Phen. IhERG was elicited by a voltage protocol

shown as lower traces, comprised of a 2s depolarizing pulse to +20 mV, followed by repolarization to -40 mV. C: Time-course of IhERG inhibition: plots of IhERG tails in control, during phenanthrene application and washout. D: Concentration response relation for phenanthrene inhibition of IhERG. Five different concentrations between 1 μM and 50 μM were tested (1 μM, 5 μM, 10 μM, 30 μM and 50 μM). At least 5 replicates per concentration were obtained. Data were fitted with equation 2. Phenanthrene inhibited IhERG carried by the hERG 1a isoform with a half-maximal inhibitory concentration (IC50) of 16.8 ± 1.7 μM, Hill coefficient of 1.0 ± 0.1.

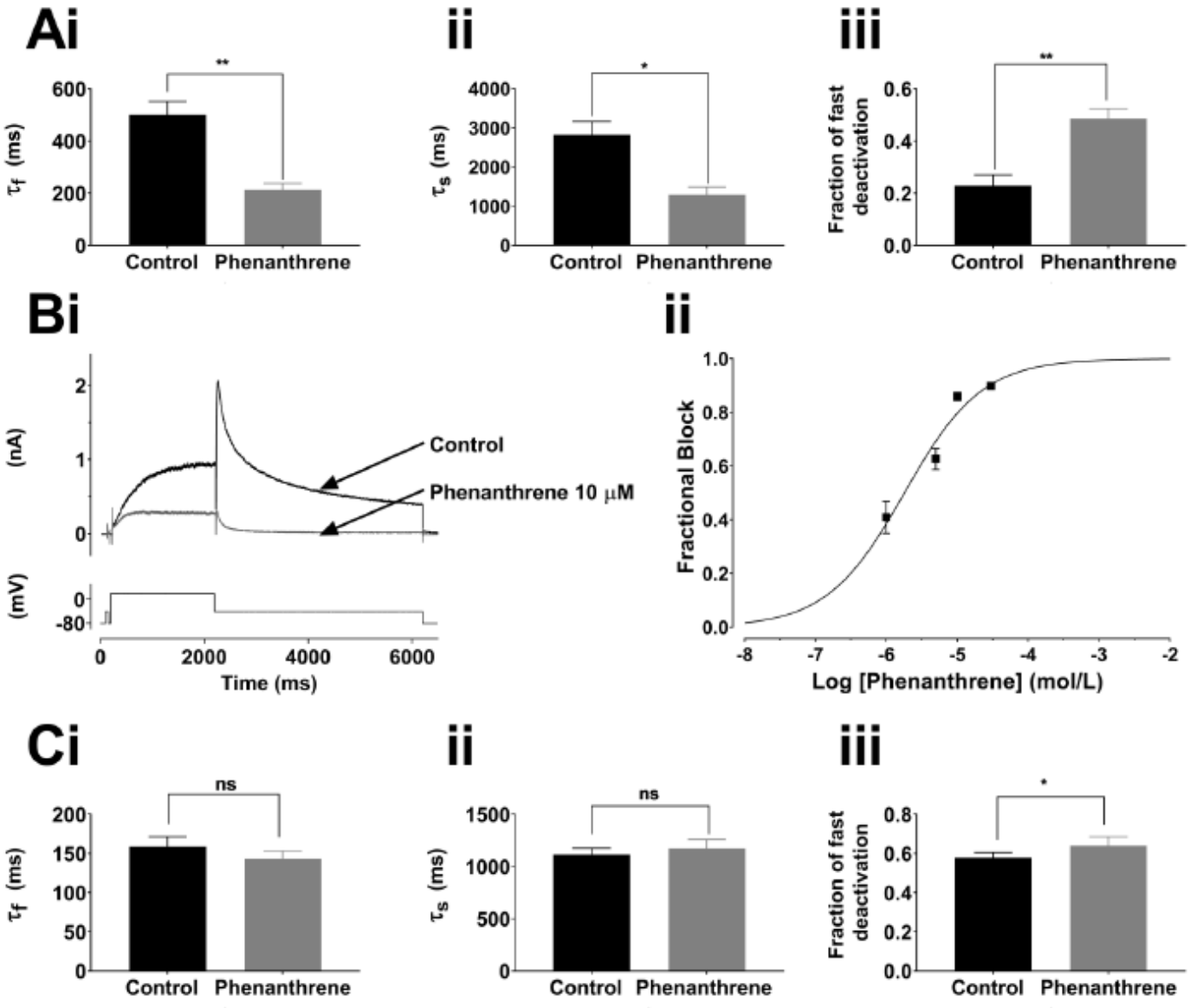

Figure 2

A: Bar charts comparing deactivation parameters for IhERG (hERG1a) tails elicited on repolarisation to 40 mV from +20 mV in Control (black), and 10 μM phenanthrene (gray). Biexponential fitting yielded fast and slow deactivation time constants (□f and □s respectively), plotted in Ai and Aii. Aiii shows that the proportion of fast deactivating current increased in phenanthrene. Significance is denoted by asterisks ** $p < 0.01$; * $p<0.05$ (n=5). B: Bi shows representative traces of hERG1a/1b IhERG elicited by the standard protocol shown in Figure 1 in the absence and presence of 10 μM phenanthrene. Bii shows concentration

response data for 4 phenanthrene concentrations (1 μM, 5 μM, 10 μM, 30 μM; n= at least 5 at each concentration). Data were fitted with equation 2, yielding a half-maximal inhibitory concentration (IC50) 1.8 ± 0.3 μM and Hill slope of 0.79 ± 0.1. C: Bar charts showing deactivation parameters for IhERG (hERG1a/1b) tails elicited on repolarisation to 40 mV from +20 mV in Control (black), and 1 μM phenanthrene (gray). Biexponential fitting yielded fast and slow deactivation time constants (□f and □s respectively), plotted in Ci and Cii. Ciii shows that the proportion of fast deactivating current increased in the presence of phenanthrene (* p <0.05 n=6).

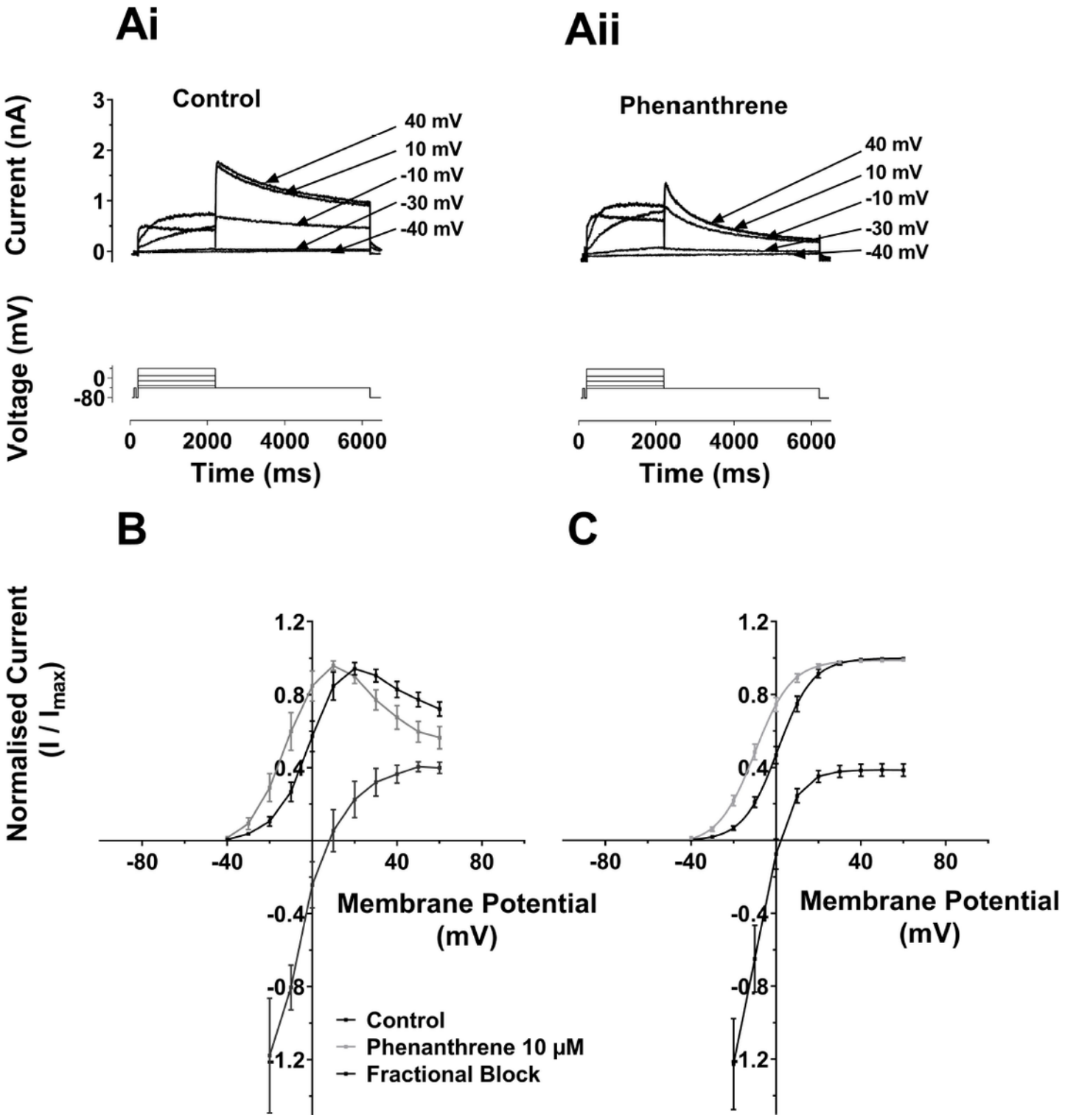

Figure 3

A: Representative IhERG traces (upper) are shown for Ai: in control solution and Aii: in 10 μM phenanthrene. IhERG was elicited by a voltage protocol (lower traces) that was comprised of 2s command pulses applied at 10 mV increments between −40 mV and +60 mV. Only selected traces are shown for clarity of display. Each current trace is labelled with its corresponding test potential. B: Mean I-V relation for end-pulse currents. Currents were normalized to the maximum current in each of control and 10 μM phenanthrene. Corresponding mean fractional inhibition by 10 μM Phenanthrene is also shown. C: Mean IhERG tails in Control (black) and phenanthrene (gray) following the different voltage commands. Currents were normalized to the maximum current in each of control and 10 μM phenanthrene Boltzmann fitting gave an activation V0.5 for Control of 1.3 ± 1.6 mV, slope: 7.2 ± 0.2 (n=16) and for phenanthrene gave a V0.5 of -8.9 ± 1.5 (p<0.001 vs Control), Slope: 7.8 ± 0.3 (n=16).

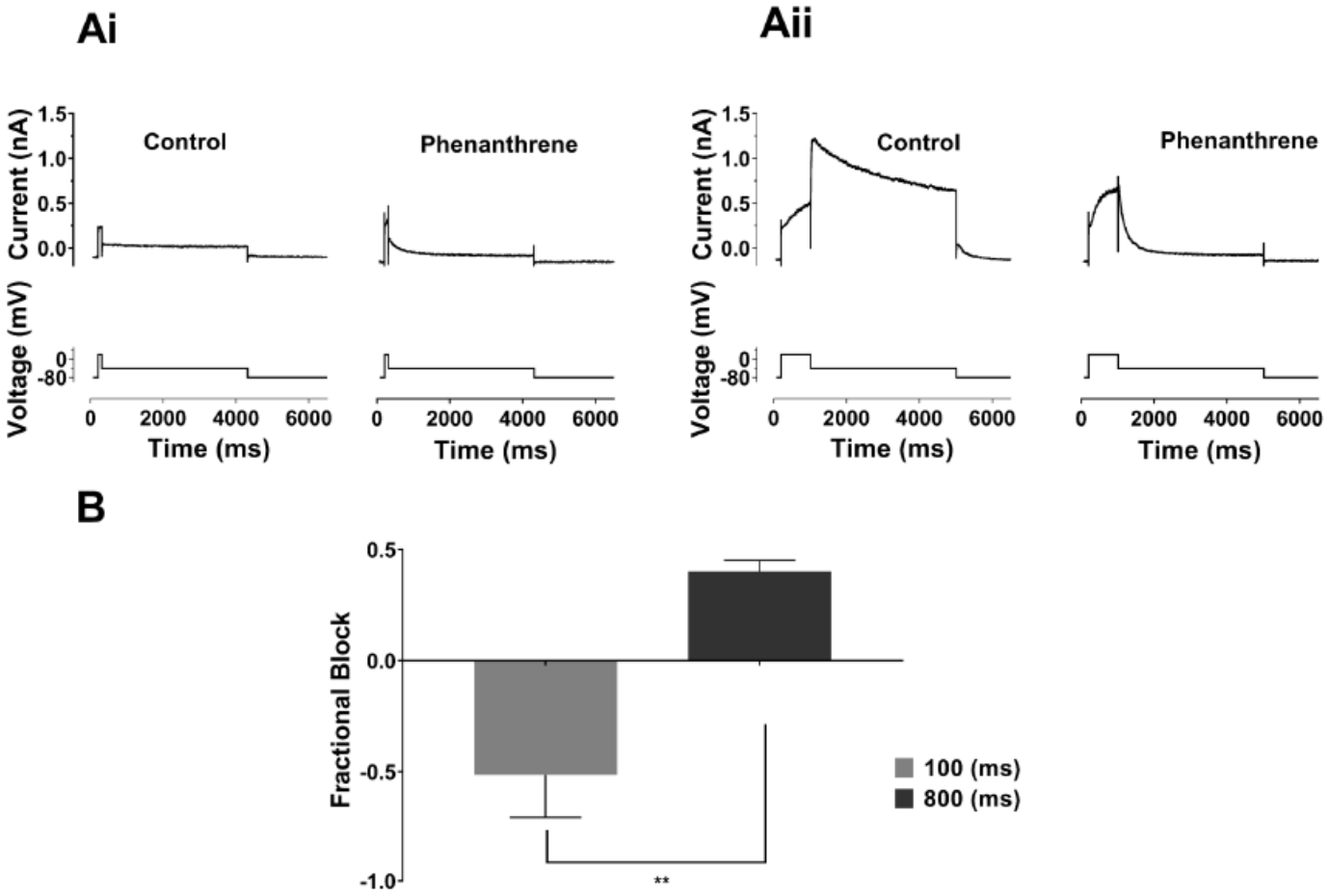

Figure 4

A: Upper traces show representative IhERG records in Control (black) and in 10 μM phenanthrene (gray). Tail currents were elicited by depolarizing to +20 mV for 100 ms in Ai and 800 ms in Aii. The voltage protocol is shown under each current trace. B Bar chart compares the mean fractional block of IhERG tail by 10 μM phenanthrene at each time-point (** p < 0.01; n=5).

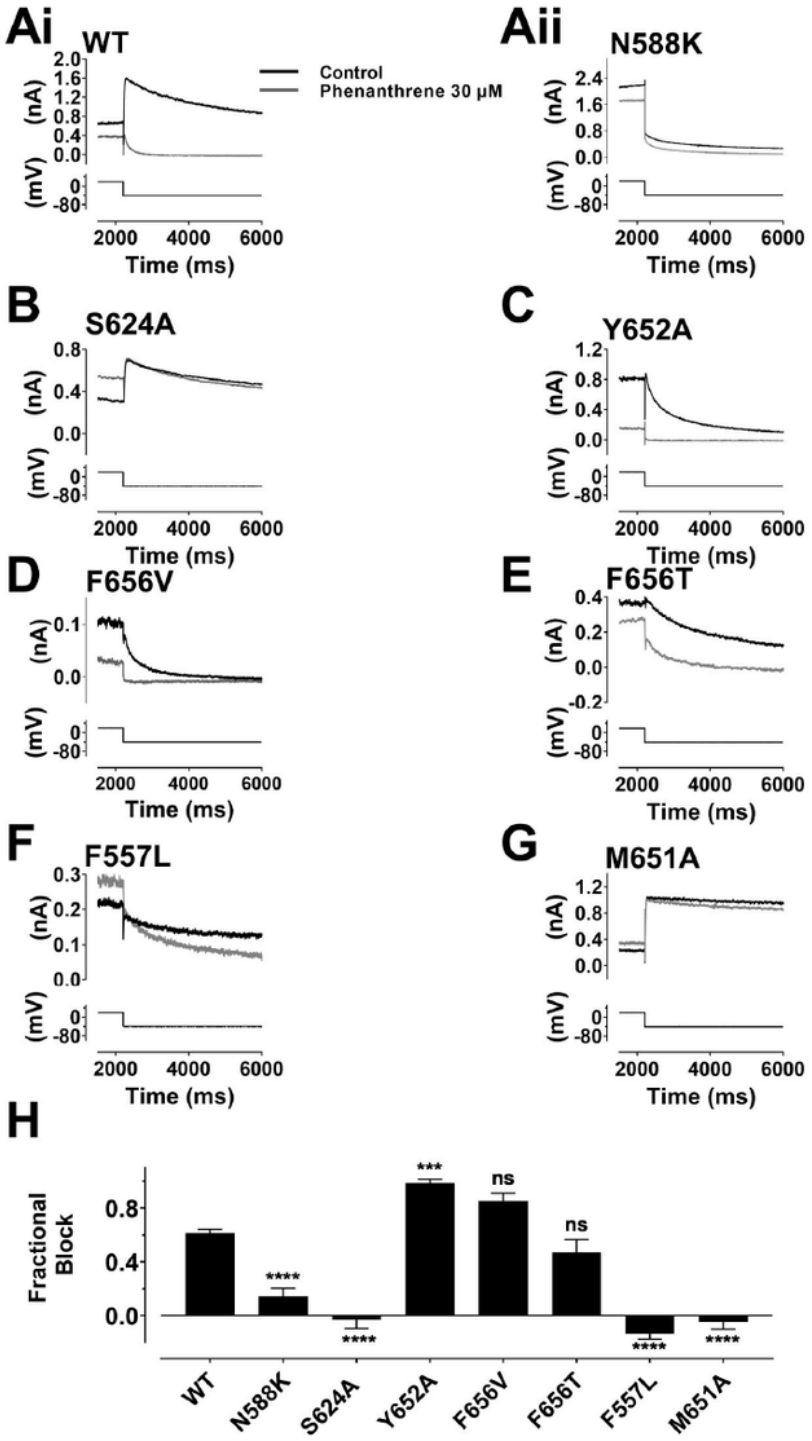

Figure 5

Effect of hERG mutations on the inhibitory effect of phenanthrene on IhERG. A – G show representative tail current traces (upper) for control IhERG (black) and during application of 30 µM Phen IhERG (gray), elicited by same voltage protocol used for Figure 1 (lower) as described. Ai: wild-type (WT), Aii: N588K, B: S624A, C: Y652A, D: F656V, E: F656V, F: F557L and G: M651A. H: Bar chart shows extent of mean tail current block by 30 µM for WT, N588K, Y652A, S624A, F656V, F656T, F557L and M651A IhERG

respectively. One way ANOVA (F= 61.2, P < 0.0001). Significance for post-hoc Bonferroni comparisons of each mutant with WT is denoted by asterisks **** p < 0.0001, *** p < 0.001 (WT n= 5, N588K n=7, Y652A n=6, S624A n= 5, F656V n= 5, F656T n= 5, F557L n=7 and M651A n=6).

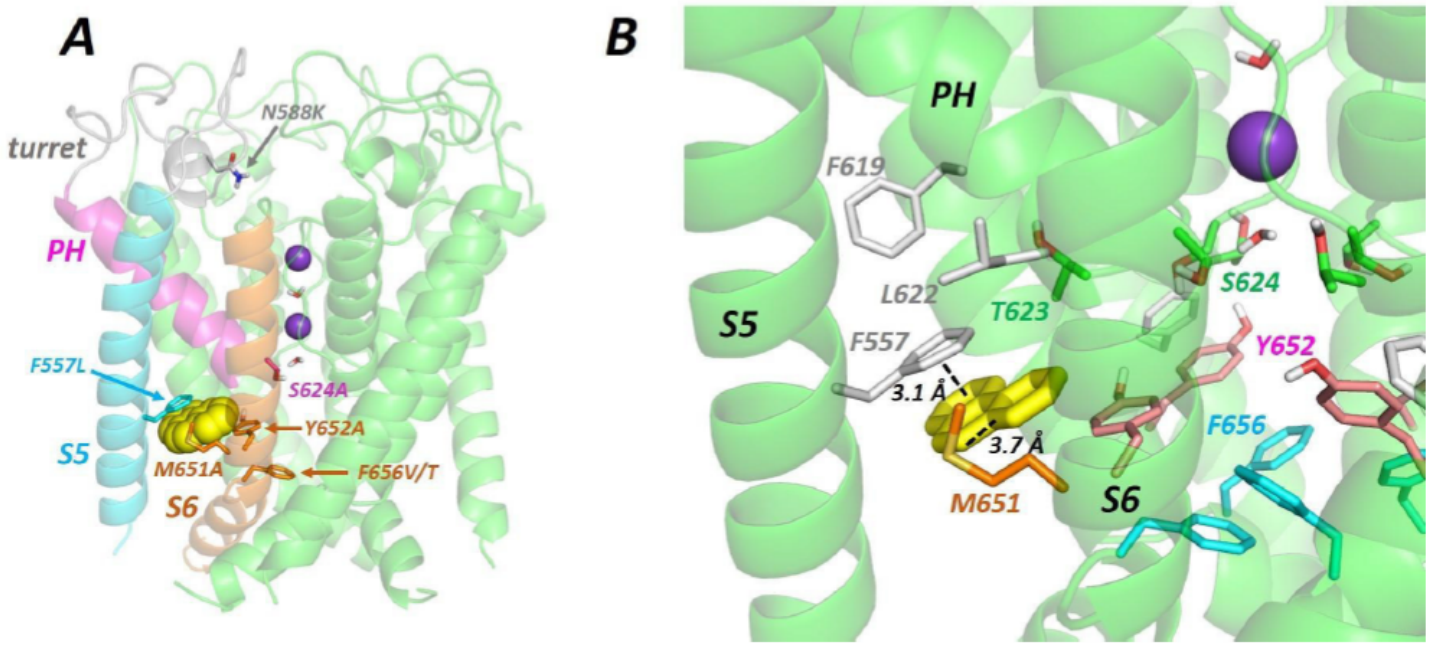

Figure 6

A: Low energy score pose for phenanthrene (yellow space-filling representation) docked into the hERG pore. The hERG subunit with docked phenanthrene shows the location within a single subunit of the mutations described in the text; the structural elements are coloured to match the alignment in Figure 1a. Purple spheres are K+ ions in the 1 and 3 positions of the selectivity filter. B: Close-up of a hydrophobic pocket containing docked phenanthrene (yellow sticks) in the same pose as panel A. An aromatic pi-stacking interaction with the F557 side chain and close interactions with the M651 side chain are indicated with dotted lines.

Supplementary Files

This is a list of supplementary files associated with this preprint. Click to download.

- AlMoubaraketalPhenanthrenehERGSupplement010721.docx